Determining elastic behavior of composites by the boundary element method

J. W. Eischen
Department of Mechanical and Aerospace Engineering, North Carolina State University, Raleigh, North Carolina 27695-7910

S. Torquato
Department of Civil Engineering and Operations Research and the Princeton Materials Institute, Princeton University, Princeton, New Jersey 08544

(Received 11 November 1992; accepted for publication 2 March 1993)

The *boundary element method* is applied to determine the effective elastic moduli of continuum models of composite materials. In this paper, we specialize to the idealized model of hexagonal arrays of infinitely long, aligned cylinders in a matrix (a model of a fiber-reinforced material) or a thin-plate composite consisting of hexagonal arrays of disks in a matrix. Thus, one need only consider two-dimensional elasticity, i.e., either plane-strain or plane-stress elasticity. This paper examines a variety of cases in which the inclusions are either stiffer or weaker than the matrix for a wide range of inclusion volume fractions ϕ_2. Our comprehensive set of simulation data for the elastic moduli are tabulated. Using the boundary element method, a key microstructural parameter η_2 that arises in rigorous three-point bounds on the effective shear modulus is also computed. Our numerical simulations of the elastic moduli for the hexagonal array are compared to rigorous two-point and three-point bounds on the respective effective properties. In the extreme instances of either superrigid particles or voids, we compare analytical relations for the elastic moduli near dilute and close packing limits to our simulation results.

I. INTRODUCTION

The problem of determining the effective transport and mechanical properties of disordered composite materials is a classical subject of research in science and engineering, dating back to the work of Maxwell,[1] Rayleigh,[2] and Einstein.[3] The complexity of the microstructure of random composite media makes an exact theoretical determination of the effective properties generally not possible. This naturally leads one to attempt to estimate the properties from partial statistical information on the sample in the form of correlation functions, and in particular, to establish the range of possible values the effective properties can take given such limited morphological information, i.e., to determine rigorous upper and lower bounds on the properties. In the last decade, considerable theoretical progress has been made on the derivation of rigorous bounds,[4–6] identification of the microstructures that correspond to the extreme values (i.e., optimal bounds),[7–10] and the systematic characterization and determination of the statistical correlation functions that arise in bounds.[11] There has been relatively much less research directed toward obtaining effective properties "exactly" from computer simulations, especially for *off-lattice* or *continuum* models (e.g., distribution of particles in a matrix). Such "*computer experiments*" could provide unambiguous tests on theories for well-defined model microstructures.

In the case of static composite media, most numerical studies have focused on obtaining effective diffusion parameters such as the effective conductivity, effective diffusion coefficient, and effective time scales associated with diffusion and reaction among traps. An efficient means of computing effective diffusion properties is by employing first-passage-time algorithms.[12] Comparatively speaking, there is a dearth of numerical simulations of the effective elastic moduli of continuum models of composites.

Approximately 20 years ago, numerical data for the effective elastic moduli were obtained for square[13,14] and hexagonal arrays[15] arrays of cylinders in a matrix for a limited selection of material properties. Most of these studies made use of finite difference procedures. Very recently, Day *et al.*[16] have devised a discretized-spring scheme that is realized on digital-image-based model of a two-dimensional, two-phase material in which one of the phases has zero elastic moduli (i.e., holes) to compute the effective elastic moduli. This method has recently been extended to treat cases in which both phases have nonzero moduli.[17]

The purpose of this paper is to begin a program to provide accurate and comprehensive numerical data for the effective elastic moduli of continuum models of composite materials by employing the *boundary element method*.[18] In the first paper of this series, we specialize to the idealized model of hexagonal arrays of infinitely long, aligned cylinders in a matrix (a model of a fiber-reinforced material) or a thin-plate composite consisting of hexagonal arrays of disks in a matrix.[13] (In the sequel to this paper, random arrays will be studied.[19]) In all cases we seek to determine the effective elastic properties in a plane perpendicular to the generators and thus need only consider two-dimensional elasticity (i.e., either plane-strain or plane-stress elasticity). We examine a number of instances in which the inclusions are either stiffer or weaker than the matrix for a wide range of inclusion volume fractions ϕ_2. Because the method is accurate, we tabulate all of the simulation data for the elastic moduli. Using the boundary

 0021-8979/93/74(1)/159/12/$6.00 © 1993 American Institute of Physics

Downloaded 08 Jul 2002 to 128.112.82.136. Redistribution subject to AIP license or copyright, see http://ojps.aip.org/japo/japcr.jsp

element method, we also compute a key microstructural parameter η_2 that arises in rigorous three-point bounds on the effective shear modulus. Our numerical simulations of the elastic moduli for the hexagonal array are compared to rigorous two-point and three-point bounds on the respective effective properties. Finally, in the extreme instances of superrigid particles or voids, we compare analytical relations for the elastic moduli near close packing to our simulation results.

The remainder of the paper is organized as follows. In Sec. II we review some pertinent theoretical results and obtain an asymptotic relation near close packing for the effective shear modulus in the case of superrigid inclusions in an incompressible matrix. In Sec. III the boundary element method is described for the problem at hand, i.e., for two-dimensional arrays of inclusions. In Sec. IV we present our simulation results for the in-plane elastic moduli of hexagonal arrays. Here we also present numerical data for the aforementioned three-point microstructural parameter η_2 arising in bounds for the shear modulus. Our data are compared to rigorous bounds and analytical asymptotic relations. Finally, in Sec. V we make concluding remarks.

II. THEORETICAL RESULTS

Here we discuss some previous theoretical results for the elastic moduli such as the dilute-concentration results, high-concentration results, and rigorous three-point bounds. In the case of nearly touching superrigid inclusions in an incompressible matrix, we derive an analytical expression for the effective shear modulus.

A. Basic definitions for two-dimensional elasticity

Before reviewing some theoretical results pertinent to this paper, it useful to define the elastic moduli for two-dimensional (2D) media. First consider a homogeneous 2D body which is isotropic. For such a material, the relationship between the stress tensor σ_{ij} and strain tensor ϵ_{ij} is given by

$$\sigma_{ij}=(k-G)\epsilon_{kk}\delta_{ij}+2G\epsilon_{ij}, \quad i,j,k=1,2. \tag{1}$$

This relation defines the 2D bulk modulus k and shear modulus G. Note that the symmetric stress and strain tensors have three independent components. Similarly, we write the strain-stress relation as

$$\epsilon_{ij}=\frac{1}{E}[(1+\nu)\sigma_{ij}\delta_{ij}-\nu\sigma_{kk}\delta_{ij}], \quad i,j,k=1,2, \tag{2}$$

where ν and E are the 2D Poisson's ratio and Young's modulus, respectively. Clearly, there are only two independent moduli. Comparing relations (1) and (2) yields, e.g., the following interrelations:

$$G=\frac{E}{2(1+\nu)}, \tag{3}$$

$$\nu=\frac{k-G}{k+G}, \tag{4}$$

$$\frac{4}{E}=\frac{1}{k}+\frac{1}{G}. \tag{5}$$

Equation (4) reveals that the 2D Poisson's ratio lies in the interval $[-1,1]$ as opposed to its three-dimensional (3D) counterpart that lies in the interval $[-1,0.5]$.

Now consider a two-phase 2D body. Denote the corresponding elastic moduli for phase i by k_i, G_i, ν_i, and E_i. Then relations (3)–(5) apply to each phase, i.e., append a subscript i to each of the moduli in Eqs. (3)–(5). Similarly, denote the corresponding 2D effective moduli by k_e, G_e, ν_e, and E_e. Again, relations (3)–(5) apply to the effective properties. The constitutive relations (1) and (2) apply as well except that the stress and strain tensors must be replaced with the *average* stress and *average* strain tensors, respectively.

Thus far we have not had to state whether we are dealing with *plane-strain* or *plane-stress* elasticity. Such specifications only arise when one desires to make contact with 3D elasticity. Plane-strain elasticity is physically relevant when considering a fiber-reinforced material. On the other hand, plane-stress elasticity is physically relevant when considering two-phase composites in the form of thin sheets. It is simple to relate 2D to 3D moduli for a single 3D isotropic material. This is done in the Appendix where it is shown, among other results, that the 2D shear modulus G (either in plane strain or plane stress) is equal to the 3D shear modulus. However, the bulk-moduli relations are not so simple. The plane-strain bulk modulus k is related to the 3D bulk modulus K by the well-known relation

$$k=K+G/3. \tag{6}$$

By contrast the plane-stress bulk modulus k obeys the relation

$$k=\frac{9KG}{3K+4G}. \tag{7}$$

Other interrelations among the 2D and 3D moduli are given in the Appendix. It is important to emphasize that the relations (6) and (7) apply only to individual phases. *Relations (6) and (7) do not apply to the effective properties.* In the Appendix we discuss the interrelations among the effective 2D moduli and the effective 3D moduli.

B. Dilute-concentration results

Consider any macroscopically isotropic 2D composite consisting of a equisized circular disks in matrix. Through first order in the inclusion volume fraction ϕ_2, the following exact asymptotic relations hold for the effective in-plane bulk and shear moduli, respectively,[20]

$$k_e=k_1+(k_2-k_1)\frac{(k_1+G_1)}{(k_2+G_1)}\phi_2, \tag{8}$$

$$G_e=G_1+\frac{2G_1(G_2-G_1)(k_1+G_1)}{G_2(k_1+G_1)+G_1(k_1+G_2)}\phi_2. \tag{9}$$

Downloaded 08 Jul 2002 to 128.112.82.136. Redistribution subject to AIP license or copyright, see http://ojps.aip.org/japo/japcr.jsp

C. Intermediate-concentration results

Using the method of "resonances," Kantor and Bergman[21] obtained expansions for the elastic moduli of hexagonal arrays in powers of ϕ_2. In the case of the effective bulk modulus k_e the expansions go up to order ϕ_2^{11}; whereas in the instance of the effective shear modulus G_e the expansion goes up to order ϕ_2^5.

D. High-concentration results

It appears that Flaherty and Keller[14] were the first to find asymptotic relations for the elastic moduli of two-dimensional, two-phase composites consisting either of circular holes ($k_2=G_2=0$) or superrigid inclusions ($G_2/G_1=\infty$) near the close-packing volume fraction ϕ_2^c. They reasoned that the elastic behavior in these extreme situations was governed by the narrow "necks" between the holes or inclusions. Flaherty and Keller specifically examined *square* arrays and found that for holes

$$G_e \sim E_e \approx c_1(\phi_2^c-\phi_2)^{1/2}, \tag{10}$$

where c_1 is a simple constant dependent upon the matrix elastic moduli and lattice geometry. Similarly, for nearly touching superrigid inclusions in a compressible matrix, they found

$$G_e \sim E_e \approx c_2(\phi_2^c-\phi_2)^{-1/2}, \tag{11}$$

where c_2 is a simple constant dependent upon the matrix elastic moduli and lattice geometry. We note here that the above result for superrigid inclusions will not hold when the matrix is *incompressible*. This is easily seen by observing that their derivation breaks down in the incompressible limit.

Recently, Day *et al.*[16] obtained corresponding asymptotic relations for holes and observed that there are generally three breakdown modes for the necks. For the hexagonal array, the microgeometry of concern in this paper, they found the following relations for the effective bulk and Young's modulus, respectively,

$$\frac{k_e}{E_1} \approx \frac{1}{2\pi\sqrt{3\phi_2^c}}(\phi_2^c-\phi_2)^{1/2}, \tag{12}$$

$$\frac{E_e}{E_1} \approx \frac{8}{3\pi\sqrt{3}(\phi_2^c)^{3/2}}(\phi_2^c-\phi_2)^{3/2}, \tag{13}$$

where E_1 is the in-plane Young's modulus of the matrix and the critical inclusion volume fraction

$$\phi_2^c=\frac{\pi}{2\sqrt{3}} \approx 0.9069. \tag{14}$$

Using the equations given immediately above and relation (5), the corresponding result for the effective shear modulus is given by

$$\frac{G_e}{G_1} \approx \frac{4(1+\nu_1)}{3\pi\sqrt{3}(\phi_2^c)^{3/2}}(\phi_2^c-\phi_2)^{3/2}. \tag{15}$$

Using a similar analysis, we can obtain an asymptotic relation for superrigid inclusions in an *incompressible matrix* near the close-packing volume fraction ϕ_2^c. Specifically, we find that

$$\frac{G_e}{G_1} \approx \frac{\pi(\phi_2^c)^{3/2}}{\sqrt{3}}(\phi_2^c-\phi_2)^{-3/2}. \tag{16}$$

Note that the critical exponent here is $-3/2$ in contrast to the exponent $-1/2$ appearing in relation (11) for a compressible matrix.

E. Rigorous bounds

Employing variational principles involving the "polarization fields," Hashin and Shtrikman[22] obtained the best possible bounds on the effective bulk and shear moduli for 3D isotropic two-phase composites given only volume fraction information. Hill[23] and Hashin[24] obtained analogous bounds on the effective transverse bulk modulus k_e and effective transverse shear modulus G_e for transversely isotropic 2D, two-phase materials. We refer to all of the aforementioned inequalities as two-point bounds since they actually incorporate up to two-point correlation function information, albeit in a trivial way. They are not stated here explicitly since they are special cases of the three-point bounds described below. It is well known that the bounds on k_e are achieved for a certain composite-cylinder assemblage.[22,24] The corresponding shear moduli bounds are, however, not realized by such assemblages. Recently, Milton,[7] Norris,[8] and Lurie and Cherkaev[9] independently showed that the Hashin–Shtrikman (or Hill–Hashin) bounds on G_e were attained by hierarchical laminates, thus demonstrating, for the first time, their optimality. In other independent work, Francfort and Murat[10] found a realization of these bounds using laminates of *finite* rank.

Employing classical variational principles, Silnutzer[25] obtained bounds on the effective 2D bulk modulus k_e and effective shear modulus G_e. Milton[5] subsequently simplified each of the above three-point bounds, showing that the bounds on k_e can be expressed in terms of ϕ_2 and a three-point parameter ζ_2 (defined below) and that the bounds on G_e can be expressed in terms of ϕ_2, ζ_2, and another three-point parameter η_2 (defined below). The simplified forms of the Silnutzer three-point bounds on the effective bulk and shear moduli are, respectively, given by

$$k_L^{(3)} \leqslant k_e \leqslant k_U^{(3)}, \tag{17}$$

$$k_L^{(3)}=\left[\langle 1/k\rangle-\frac{\phi_1\phi_2(1/k_2-1/k_1)^2}{\langle 1/\tilde{k}\rangle+\langle 1/G\rangle_\zeta}\right]^{-1}, \tag{18}$$

$$k_U^{(3)}=\left[\langle k\rangle-\frac{\phi_1\phi_2(k_2-k_1)^2}{\langle \tilde{k}\rangle+\langle G\rangle_\zeta}\right], \tag{19}$$

and

$$G_L^{(3)} \leqslant G_e \leqslant G_U^{(3)}, \tag{20}$$

$$G_L^{(3)}=\left[\langle 1/G\rangle-\frac{\phi_1\phi_2(1/G_2-1/G_1)^2}{\langle 1/\tilde{G}\rangle+\Xi}\right]^{-1}, \tag{21}$$

Downloaded 08 Jul 2002 to 128.112.82.136. Redistribution subject to AIP license or copyright, see http://ojps.aip.org/japo/japcr.jsp

$$G_U^{(3)}=\left[\langle G\rangle-\frac{\phi_1\phi_2(G_2-G_1)^2}{\langle\widetilde{G}\rangle+\Theta}\right], \tag{22}$$

where

$$\Theta=\frac{[2\langle k\rangle_\zeta\langle G\rangle^2+\langle k\rangle^2\langle G\rangle_\eta]}{\langle k+2G\rangle^2}, \tag{23}$$

$$\Xi=2\langle 1/k\rangle_\zeta+\langle 1/G\rangle_\eta, \tag{24}$$

$$\langle b\rangle=b_1\phi_1+b_2\phi_2, \tag{25}$$

$$\langle\widetilde{b}\rangle=b_1\phi_2+b_2\phi_1, \tag{26}$$

$$\langle b\rangle_\zeta=b_1\zeta_1+b_2\zeta_2, \tag{27}$$

$$\langle b\rangle_\eta=b_1\eta_1+b_2\eta_2, \tag{28}$$

and

$$\zeta_1=1-\zeta_2, \tag{29}$$

$$\zeta_2=\frac{4}{\pi\phi_1\phi_2}\int_0^\infty\frac{dr}{r}\int_0^\infty\frac{ds}{s}\int_0^\pi d\theta\cos(2\theta)\left[S_3(r,s,t)-\frac{S_2(r)S_2(s)}{\phi_2}\right], \tag{30}$$

$$\eta_1=1-\eta_2, \tag{31}$$

$$\eta_2=\frac{16}{\pi\phi_1\phi_2}\int_0^\infty\frac{dr}{r}\int_0^\infty\frac{ds}{s}\int_0^\pi d\theta\cos(4\theta)\left[S_3(r,s,t)-\frac{S_2(r)S_2(s)}{\phi_2}\right]. \tag{32}$$

For isotropic media, the n-point probability functions S_n depend upon the relative distances of the n points. $S_2(r)$ is the probability of finding in phase 2 the endpoints of a line segment of length r. $S_3(r,s,t)$ is the probability of finding in phase 2 the vertices of a triangle with sides of lengths r, s, and t, when randomly thrown into the sample. Here θ is the angle opposite the side of the triangle with length t. That ζ_i and η_i must lie in the closed interval [0,1] implies that the bounds (17) and (20) always improve upon the Hill–Hashin two-point bounds. When $\zeta_2=0$ and $\eta_2=0$, the bounds (17) and (20) coincide and equal the corresponding two-point Hill–Hashin lower bounds (for $k_2\geqslant k_1$ and $G_2\geqslant G_1$). When $\zeta_2=1$ and $\eta_2=1$, the bounds (17) and (20) coincide and equal the corresponding Hill–Hashin upper bounds (for $k_2\geqslant k_1$ and $G_2\geqslant G_1$). It is important to emphasize that the three-point bounds (17) and (20) are valid for *any* isotropic microgeometry.

Note that when the phase shear moduli are equal ($G_1=G_2=G$), the bounds (17) and (20) collapse, i.e., they yield the exact results:

$$G_e=G, \tag{33}$$

$$k_e=k_1+\frac{\phi_2}{[1/(k_2-k_1)]+[\phi_1/(k_1+G)]}. \tag{34}$$

This result, which was first shown by Hill,[22] will be used to test our simulation results. Recently, Thorpe and Jasiuk[26] have noted that the exact results (33) and (34) are equivalent to stating that both the effective Poisson's ratio and Young's modulus obey the law of mixtures.

III. BOUNDARY ELEMENT METHOD

The boundary element method (BEM) provides a very efficient way to compute effective elastic properties of fiber reinforced composite materials. The elastic inclusion boundary value problems described in the following section must be solved to determine the relationship between certain fundamental strain states and corresponding average stress measures. The BEM is ideally suited for this because all information regarding effective properties is accessible on the boundary of the elastic domain, no interior field data is required.

A. Basic equations

The boundary integral equation for linear elasticity is[18]

$$c_{ij}(\xi)u_j(\xi)+\int_\Gamma p_{ij}^*(\xi,\mathbf{x})u_j(\mathbf{x})d\Gamma(\mathbf{x})=\int_\Gamma u_{ij}^*(\xi,\mathbf{x})p_j(\mathbf{x})d\Gamma(\mathbf{x}), \tag{35}$$

where $\Gamma(\xi)$ represents the bounding curve (including inclusion boundaries) of the elastic problem. The displacement components on the boundary are u_j and traction components are p_j. Summation is implied over repeated subindices. This integral equation must be satisfied at each "source" point ξ on the boundary. Note that ξ is a vector with two measure numbers (ξ_1,ξ_2) referred to an arbitrary origin. The "field" point position vector has measure numbers (x_1,x_2). The quantities p_{ij}^* and u_{ij}^* are related to the Green's function for 2D linear isotropic elasticity and are given by

$$u_{ij}^*(\xi,\mathbf{x})=\frac{1}{8\pi(1-\nu)G}\left[(3-4\nu)\log\left(\frac{1}{r}\right)\delta_{ij}+r_{,i}r_{,j}\right], \tag{36}$$

$$p_{ij}^*(\xi,\mathbf{x})=-\frac{1}{4\pi(1-\nu)r}\left([(1-2\nu)\delta_{ij}+2r_{,i}r_{,j}]\frac{\partial r}{\partial n}-(1-2\nu)(r_{,i}n_j-r_{,j}n_i)\right) \tag{37}$$

for an isotropic material and the plane strain condition. G is the transverse shear modulus and ν is Poisson's ratio. In this context, G and ν are the 3D material properties. For generalized plane stress replace ν by $\nu/1+\nu$. Other quantities appearing in these expressions are defined by

$$r\equiv(r_ir_i)^{1/2}, \tag{38}$$

$$r_i\equiv x_i-\xi_i, \tag{39}$$

$$r_{,i}\equiv\frac{\partial r}{\partial x_i}=\frac{r_i}{r}, \tag{40}$$

$$\frac{\partial r}{\partial n}=\frac{\partial r}{\partial x_i}n_i=\frac{r_in_i}{r}\quad\text{(directional derivative)}. \tag{41}$$

Downloaded 08 Jul 2002 to 128.112.82.136. Redistribution subject to AIP license or copyright, see http://ojps.aip.org/japo/japcr.jsp

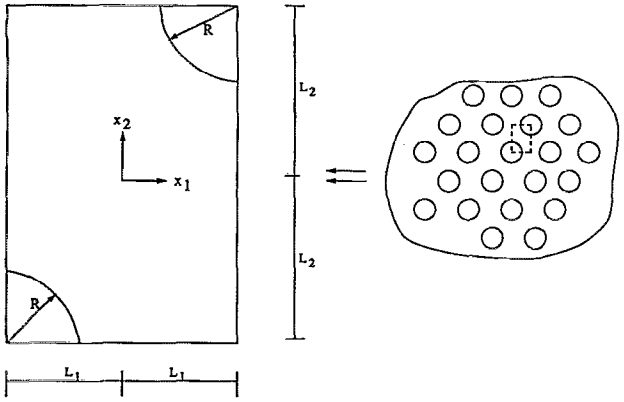

FIG. 1. Unit cell for hexagonal array BEM computations.

Note that n_i are the measure numbers of the unit outward normal vector to the bounding curve Γ. The tensor $u_{ij}^*(\xi,\mathbf{x})$ represents the displacement in direction j at field point $\mathbf{x}$ due to a unit force applied in direction i at the source point ξ, while tensor $p_{ij}^*(\xi,\mathbf{x})$ represents the traction in direction j at field point $\mathbf{x}$ due to a unit force applied in direction i at the source point ξ. The tensor c_{ij} is determined by requiring that rigid body displacements yield zero tractions. The values are computed numerically during formation of the discrete boundary element equation.

For the composite problem, the boundary element equation is enforced along the matrix external boundary, the fiber external boundary, and matrix/fiber interfaces (see discussion of unit cell in Sec. IV). Continuity of displacement and traction are enforced along all matrix-fiber interfaces. Several notes regarding the numerical methods used to solve the boundary element equation are in order.

(1) Becker[18] provides a comprehensive treatment of the numerical solution of the boundary element equation, including treatment of inclusions.

(2) Corner points have been treated by allowing two independent displacement components and *four* independent traction components. No "rounding of corners" or "double-noding with small separation distance" has been used.

(3) The logarithmic singularity in u_{ij}^* was integrated analytically to avoid numerical error.

(4) Three node quadratic elements were employed along with eight-point Gaussian integration.

B. Unit cell and loading for hexagonal array

Figure 1 shows the unit cell employed for the hexagonal array configuration. Numerous choices exist for the unit cell geometry. The one we selected is extremely convenient for specification of boundary stresses and displacements. The unit cell is rectangular in shape with dimension $2L_1\times 2L_2$, with $L_2=\sqrt{3}L_1$. Two quarter circular elastic inclusions (fibers) of radius R are shown. Cartesian coordinates fixed at the center of the cell parameterize position. The fiber volume fraction ϕ_2 is related to the cell geometry according to

$$\phi_2=\frac{\pi}{2\sqrt{3}}\left(\frac{R}{L}\right)^2, \tag{42}$$

where $L^2=(L_1)^2+(L_2)^2$ is the half-length of the unit cell diagonal. Note that $R/L=1$ corresponds to the critical inclusion volume fraction.

The two dimensional effective bulk and shear moduli were calculated by solving two fundamental boundary value problems with imposed average stress and strain. The strains for the first problem were $\bar{\epsilon}_{11}=0$, $\bar{\epsilon}_{22}=1$ with $\bar{\sigma}_{12}=0$. Area average strain and stress quantities are defined according to

$$\bar{\epsilon}_{ij}=\frac{1}{4L_1L_2}\int_{-L_2}^{L_2}\int_{-L_1}^{L_1}\epsilon_{ij}(x_1,x_2)dx_1\,dx_2,$$

$$\bar{\sigma}_{ij}=\frac{1}{4L_1L_2}\int_{-L_2}^{L_2}\int_{-L_1}^{L_1}\sigma_{ij}(x_1,x_2)dx_1\,dx_2. \tag{43}$$

It is straightforward to show using the strain displacement equations and divergence theorem that the appropriate displacement and stress boundary conditions on the unit cell are

$$u_2(x_1,L_2)/L_2=-u_2(x_1,-L_2)/L_2=1,$$

$$u_1(-L_1,x_2)=u_1(L_1,x_2)=0, \tag{44}$$

$$\sigma_{12}(x_1,L_2)=\sigma_{12}(x_1,-L_2)$$

$$=\sigma_{12}(-L_1,x_2)=\sigma_{12}(L_1,x_2)=0. \tag{45}$$

Using the stress equilibrium equations and the divergence theorem, it can be shown that the average stress $\bar{\sigma}_{22}$ can be expressed as

$$\bar{\sigma}_{22}=\frac{1}{2L_1}\int_{-L_1}^{L_1}\sigma_{22}(x_1,L_2)dx_1. \tag{46}$$

Since the boundary element method naturally provides data (i.e., σ_{22}) on the boundary of the unit cell, this definition of $\bar{\sigma}_{22}$ was employed rather than Eq. (43). Then, Eq. (1) provides the relationship for the difference between the effective bulk and shear moduli

$$k_e-G_e=\bar{\sigma}_{22}. \tag{47}$$

The second fundamental problem was an imposed average shear strain $\bar{\epsilon}_{12}=1/2$ with $\bar{\sigma}_{11}=\bar{\sigma}_{22}=0$. The displacement and stress boundary conditions in this case are

$$u_1(x_1,L_2)/L_2=-u_1(x_1,-L_2)/L_2=1,$$

$$u_2(-L_1,x_2)=u_2(L_1,x_2)=0, \tag{48}$$

$$\sigma_{22}(x_1,L_2)=\sigma_{22}(x_1,-L_2)$$

$$=\sigma_{11}(-L_1,x_2)=\sigma_{11}(L_1,x_2)=0. \tag{49}$$

Again, the average shear stress can be expressed in terms of a boundary integral

$$\bar{\sigma}_{12}=\frac{1}{2L_1}\int_{-L_1}^{L_1}\sigma_{12}(x_1,L_2)dx_1. \tag{50}$$

Equation (1) then yields

Downloaded 08 Jul 2002 to 128.112.82.136. Redistribution subject to AIP license or copyright, see http://ojps.aip.org/japo/japcr.jsp

$$G_e=\bar{\sigma}_{12}. \tag{51}$$

It is then a simple matter to calculate k_e using Eq. (47).

IV. RESULTS AND DISCUSSION

A. Microstructural parameter η_2

The microstructural parameter η_2 was calculated approximately using the boundary element method and the three-point bound formulas for the effective shear modulus in the incompressible limit $k_1=k_2=\infty$, i.e.,

$$G_L^{(3)}=\left(\langle 1/G\rangle-\frac{\phi_1\phi_2(1/G_2-1/G_1)^2}{\langle 1/\tilde{G}\rangle+\langle 1/G\rangle_\eta}\right)^{-1}, \tag{52}$$

$$G_U^{(3)}=\langle G\rangle-\frac{\phi_1\phi_2(G_2-G_1)^2}{\langle \tilde{G}\rangle+\langle G\rangle_\eta}. \tag{53}$$

Each of these equations can be solved for η_2 as

$$\eta_2=\left(\frac{\phi_1\phi_2(1/G_2-1/G_1)^2}{\langle 1/G\rangle-1/G_L^{(3)}}-\langle 1/\tilde{G}\rangle-\frac{1}{G_1}\right)\Bigg/\left(\frac{1}{G_2}-\frac{1}{G_1}\right) \quad \text{(lower bound)}, \tag{54}$$

$$\eta_2=\left(\frac{\phi_1\phi_2(G_2-G_1)^2}{\langle G\rangle-G_U^{(3)}}-\langle \tilde{G}\rangle-G_1\right)\Bigg/(G_2-G_1) \quad \text{(upper bound)}. \tag{55}$$

Simulations were performed for the hexagonal array geometry at various volume fractions and with shear modulus ratios G_2/G_1 slightly greater than 1. The effective shear modulus G_e was determined precisely as described in Sec. III B. Lower and upper bound estimates for η_2 (η_2^L and η_2^U) were calculated using Eqs. (55) and (54), respectively, by setting $G_U^{(3)}=G_e$ and $G_L^{(3)}=G_e$. Curves were then constructed of η_2^U vs G_2/G_1 and η_2^L vs G_2/G_1. These curves were then extrapolated back to $G_2/G_1=1$ to provide an estimate of η_2. In all cases the lower bound and upper bound curves yielded the same extrapolated value for η_2. This was expected as the bounds collapse as $G_2/G_1\to 1$. The solid circles in Fig. 2 show the result of this calculation. Note that $\eta_2\approx 0$ until ϕ_2 exceeeds 0.25, reminiscent of the behavior of ζ_2. In order to check our method, we calculated the microstructural paramemter ζ_2 in a similiar way using the lower and upper bound formulas for the effective bulk modulus [see Eqs. (18) and (19)]. Figure 2 shows the comparison between our numerical results and results reported by McPhedran and Milton.[27] The agreement is extremely good, thus providing confidence in the new results for η_2. Although both η_2 and ζ_2 are monotonically increasing functions of ϕ_2, the curvature of η_2 (unlike that of ζ_2), changes with increasing ϕ_2. Moreover, we see that η_2 is always greater or equal to ζ_2, which is consistent with the observation of Torquato[6] that there are a large class of composites for which $\eta_2\geqslant\zeta_2$. We have used the η_2 results to compute three-point bounds for comparison with all our simulations reported on in the Sec. IV B.

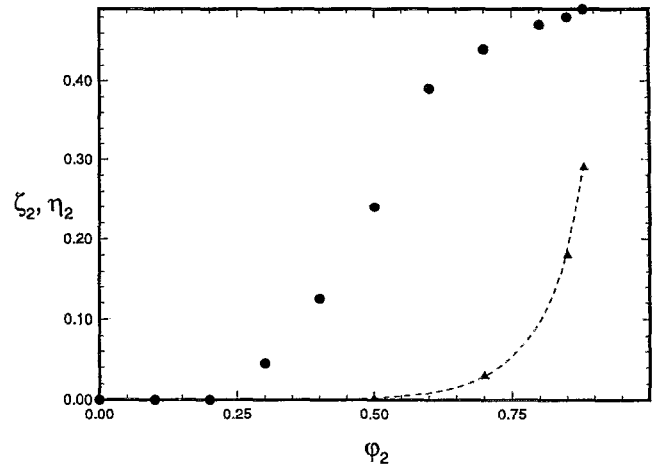

FIG. 2. Microstructural parameters ζ_2 and η_2 for hexagonal array of cylinders vs cylinder volume fraction ϕ_2; --- McPhedran and Milton (Ref. 27) for ζ_2. The black circles are the BEM results for η_2. The black triangles are BEM results for ζ_2.

The boundary element mesh that was used to generate the results discussed above consisted of 926 nodal points, with 181 nodes distributed along each of the sides $x_1=\pm L_1$, 161 nodes distributed along each of the sides $x_2=\pm L_2$, and 121 nodes distributed along each of the inclusion boundaries. This mesh yielded what were regarded as converged results based on results from two coarser meshes.

B. Effective elastic properties

As stated in Sec. I, the primary purpose of this paper is to document accurate effective elastic properties for a composite material consisting of hexagonal arrays of circular fibers embedded in a matrix. In Tables I–IX we present results for nine different matrix/fiber material property combinations at volume fractions in the range $0\leqslant\phi_2\leqslant 0.85$. Reported at the top of each table are the 3D elastic moduli for the constituents and the corresponding 2D moduli. Tables I–VII correspond to elastic inclusions either stiffer or weaker than the matrix for plane strain conditions. In particular, Tables I and V are for cases in which the fibers are superrigid relative to the matrix ($G_2/G_1=\infty$). Tables II–IV represent material properties for boron-epoxy, glass-epoxy, and boron-aluminum composites, respectively. Table VI represents a test case for the simulation. Table VII represents the case of an incompressible disk with zero shear modulus, i.e. a model of an imbedded inviscid fluid. Tables VIII–IX are for circular holes in a matrix for plane stress conditions. Boundary element numerical results for k_e/k_1, G_e/G_1, ν_e and E_e/E_1 are listed along with three-point bounds for the effective bulk modulus and effective shear modulus. Note that the three point bounds on the effective shear modulus have not been reported before in the literature for the hexagonal array because the microstructural parameter η_2 was unavailable. The results in the tables are accurate to the number of digits presented, based

Downloaded 08 Jul 2002 to 128.112.82.136. Redistribution subject to AIP license or copyright, see http://ojps.aip.org/japo/japcr.jsp

TABLE I. Material case 1, plane strain.

$G_2/G_1=\infty$, $G_1/K_1=0.46$, $G_2/K_2=0.46$, $\nu_1=0.30$, $\nu_2=0.30$ (3D Moduli) $G_2/G_1=\infty$, $G_1/k_1=0.4$, $G_2/k_2=0.4$, $\nu_1=0.43$, $\nu_2=0.43$ (2D Moduli) ϕ_2	$k_L^{(3)}/k_1$	k_e/k_1	$k_U^{(3)}/k_1$	$G_L^{(3)}/G_1$	G_e/G_1	$G_U^{(3)}/G_1$	ν_e	E_e/E_1
0.1	1.16	1.16	1.16	1.17	1.17	2.88	0.42	1.17
0.2	1.35	1.35	1.41	1.39	1.39	155	0.42	1.38
0.3	1.60	1.60	2.95	1.67	1.68	586	0.41	1.65
0.4	1.93	1.93	15.6	2.06	2.08	2426	0.40	2.04
0.5	2.40	2.40	96.5	2.64	2.69	6498	0.38	2.60
0.6	3.11	3.11	526	3.57	3.69	14073	0.36	3.50
0.7	4.30	4.33	2660	5.08	5.54	22610	0.32	5.13
0.8	6.78	7.15	13213	8.20	10.0	36698	0.28	8.99
0.85	9.46	11.0	28558	11.5	16.3	48044	0.26	14.3

TABLE II. Material case 2, plane strain.

$G_2/G_1=135$, $G_1/K_1=0.33$, $G_2/K_2=0.75$, $\nu_1=0.35$, $\nu_2=0.20$ (3D Moduli) $G_2/G_1=135$, $G_1/k_1=0.3$, $G_2/k_2=0.6$, $\nu_1=0.54$, $\nu_2=0.25$ (2D Moduli) ϕ_2	$k_L^{(3)}/k_1$	k_e/k_1	$k_U^{(3)}/k_1$	$G_L^{(3)}/G_1$	G_e/G_1	$G_U^{(3)}/G_1$	ν_e	E_e/E_1
0.1	1.14	1.14	1.14	1.18	1.18	1.19	0.53	1.17
0.2	1.32	1.32	1.32	1.40	1.40	1.56	0.52	1.38
0.3	1.54	1.54	1.54	1.69	1.70	2.23	0.50	1.66
0.4	1.84	1.84	1.85	2.10	2.11	4.27	0.49	2.04
0.5	2.25	2.25	2.34	2.69	2.75	8.52	0.46	2.62
0.6	2.86	2.87	3.34	3.65	3.81	16.5	0.43	3.54
0.7	3.87	3.90	6.16	5.18	5.74	26.3	0.39	5.18
0.8	5.85	6.12	16.1	8.20	10.2	44.1	0.33	8.82
0.85	7.82	8.87	27.7	11.3	15.6	59.5	0.31	13.3

TABLE III. Material case 3, plane strain.

$G_2/G_1=22.5$, $G_1/K_1=0.33$, $G_2/K_2=0.75$, $\nu_1=0.35$, $\nu_2=0.20$ (3D Moduli) $G_2/G_1=22.5$, $G_1/k_1=0.3$, $G_2/k_2=0.6$, $\nu_1=0.54$, $\nu_2=0.25$ (2D Moduli) ϕ_2	$k_L^{(3)}/k_1$	k_e/k_1	$k_U^{(3)}/k_1$	$G_L^{(3)}/G_1$	G_e/G_1	$G_U^{(3)}/G_1$	ν_e	E_e/E_1
0.1	1.13	1.13	1.13	1.17	1.17	1.17	0.53	1.16
0.2	1.28	1.28	1.28	1.37	1.37	1.40	0.51	1.35
0.3	1.47	1.47	1.47	1.63	1.64	1.72	0.50	1.60
0.4	1.71	1.71	1.72	1.99	2.00	2.29	0.48	1.93
0.5	2.04	2.04	2.05	2.49	2.53	3.23	0.46	2.40
0.6	2.48	2.49	2.53	3.25	3.34	4.75	0.42	3.10
0.7	3.14	3.16	3.34	4.37	4.66	6.62	0.39	4.20
0.8	4.23	4.32	4.98	6.29	7.02	9.61	0.35	6.13
0.85	5.10	5.36	6.41	7.92	9.06	11.9	0.33	7.81

TABLE IV. Material case 4, plane strain.

$G_2/G_1=6.75$, $G_1/K_1=0.33$, $G_2/K_2=0.75$, $\nu_1=0.35$, $\nu_2=0.20$ (3D Moduli) $G_2/G_1=6.75$, $G_1/k_1=0.3$, $G_2/k_2=0.6$, $\nu_1=0.54$, $\nu_2=0.25$ (2D Moduli) ϕ_2	$k_L^{(3)}/k_1$	k_e/k_1	$k_U^{(3)}/k_1$	$G_L^{(3)}/G_1$	G_e/G_1	$G_U^{(3)}/G_1$	ν_e	E_e/E_1
0.1	1.09	1.09	1.09	1.14	1.14	1.14	0.52	1.13
0.2	1.19	1.19	1.19	1.30	1.30	1.31	0.51	1.27
0.3	1.31	1.31	1.31	1.50	1.50	1.52	0.49	1.45
0.4	1.45	1.45	1.45	1.75	1.76	1.80	0.47	1.67
0.5	1.62	1.62	1.62	2.08	2.09	2.18	0.44	1.96
0.6	1.82	1.82	1.83	2.51	2.54	2.69	0.41	2.33
0.7	2.08	2.08	2.09	3.07	3.14	3.29	0.38	2.81
0.8	2.40	2.41	2.44	3.84	3.94	4.10	0.34	3.44
0.85	2.60	2.62	2.66	4.36	4.47	4.63	0.32	3.84

Downloaded 08 Jul 2002 to 128.112.82.136. Redistribution subject to AIP license or copyright, see http://ojps.aip.org/japo/japcr.jsp

TABLE V. Material case 5, plane strain.

$G_2/G_1=\infty$, $G_1/K_1=0$, $G_2/K_2=0$, $\nu_1=0.50$, $\nu_2=0.50$ (3D Moduli)
$G_2/G_1=\infty$, $G_1/k_1=0$, $G_2/k_2=0$, $\nu_1=1.0$, $\nu_2=1.0$ (2D Moduli)

ϕ_2	$k_L^{(3)}/k_1$	k_e/k_1	$k_U^{(3)}/k_1$	$G_L^{(3)}/G_1$	G_e/G_1	$G_U^{(3)}/G_1$	ν_e	E_e/E_1
0.1	...	...	...	1.22	1.22	6.77	1.00	1.22
0.2	...	...	...	1.51	1.51	489	1.00	1.51
0.3	...	...	...	1.88	1.90	1814	1.00	1.90
0.4	...	...	...	2.43	2.52	6898	1.00	2.52
0.5	...	...	...	3.32	3.66	16218	1.00	3.66
0.6	...	...	...	4.96	6.10	29622	1.00	6.10
0.7	...	...	...	7.50	12.7	41622	1.00	12.7
0.8	...	...	...	12.5	41.7	56120	1.00	41.7
0.85	...	...	...	17.6	120	64763	1.00	120

TABLE VI. Material case 6, plane strain.

$G_2/G_1=1$, $G_1/K_1=1$, $G_2/K_2=0$, $\nu_1=0.125$, $\nu_2=0.50$ (3D Moduli)
$G_2/G_1=1$, $G_1/k_1=0.75$, $G_2/k_2=0$, $\nu_1=0.14$, $\nu_2=1.0$ (2D Moduli)

ϕ_2	$k_L^{(3)}/k_1$	k_e/k_1	$k_U^{(3)}/k_1$	$G_L^{(3)}/G_1$	G_e/G_1	$G_U^{(3)}/G_1$	ν_e	E_e/E_1
0.1	1.19	1.19	1.19	1.00	1.00	1.00	0.23	1.07
0.2	1.44	1.44	1.44	1.00	1.00	1.00	0.31	1.15
0.3	1.75	1.75	1.75	1.00	1.00	1.00	0.40	1.22
0.4	2.17	2.17	2.17	1.00	1.00	1.00	0.49	1.30
0.5	2.75	2.75	2.75	1.00	1.00	1.00	0.57	1.37
0.6	3.62	3.62	3.62	1.00	1.00	1.00	0.66	1.45
0.7	5.08	5.08	5.08	1.00	1.00	1.00	0.74	1.52
0.8	8.00	8.00	8.00	1.00	1.00	1.00	0.83	1.60
0.85	10.9	10.9	10.9	1.00	1.00	1.00	0.87	1.64

TABLE VII. Material case 7, plane stress.

$G_2/G_1=0$, $G_1/K_1=0$, $G_2/K_2=0$, $\nu_1=0.50$, $\nu_2=0.50$ (3D Moduli)
$G_2/G_1=0$, $G_1/k_1=0$, $G_2/k_2=0$, $\nu_1=0.5$, $\nu_2=0.5$ (2D Moduli)

ϕ_2	$k_L^{(3)}/k_1$	k_e/k_1	$k_U^{(3)}/k_1$	$G_L^{(3)}/G_1$	G_e/G_1	$G_U^{(3)}/G_1$	ν_e	E_e/E_1
0.1	...	...	...	0.018	0.818	0.818	1.00	0.818
0.2	...	...	...	0.000	0.664	0.664	1.00	0.664
0.3	...	...	...	0.000	0.526	0.533	1.00	0.526
0.4	...	...	...	0.000	0.396	0.412	1.00	0.396
0.5	...	...	...	0.000	0.273	0.302	1.00	0.273
0.6	...	...	...	0.000	0.164	0.202	1.00	0.164
0.7	...	...	...	0.000	0.079	0.133	1.00	0.079
0.8	...	...	...	0.000	0.024	0.080	1.00	0.024
0.85	...	...	...	0.000	0.008	0.057	1.00	0.008

TABLE VIII. Material case 8, plane stress.

$G_2/G_1=0$, $G_1/K_1=0$, $G_2/K_2=1.5$, $\nu_1=0.50$, $\nu_2=0.0$ (3D Moduli)
$G_2/G_1=0$, $G_1/k_1=0.33$, $G_2/k_2=1.0$, $\nu_1=0.50$, $\nu_2=0.0$ (2D Moduli)

ϕ_2	$k_L^{(3)}/k_1$	k_e/k_1	$k_U^{(3)}/k_1$	$G_L^{(3)}/G_1$	G_e/G_1	$G_U^{(3)}/G_1$	ν_e	E_e/E_1
0.1	0.684	0.692	0.692	0.026	0.771	0.771	0.46	0.750
0.2	0.199	0.500	0.500	0.000	0.597	0.599	0.43	0.570
0.3	0.014	0.368	0.368	0.000	0.455	0.462	0.42	0.430
0.4	0.002	0.273	0.273	0.000	0.330	0.349	0.43	0.313
0.5	0.000	0.200	0.200	0.000	0.220	0.253	0.46	0.214
0.6	0.000	0.141	0.142	0.000	0.128	0.173	0.54	0.131
0.7	0.000	0.094	0.095	0.000	0.060	0.115	0.65	0.066
0.8	0.000	0.052	0.055	0.000	0.018	0.067	0.79	0.022
0.85	0.000	0.033	0.036	0.000	0.006	0.047	0.88	0.008

Downloaded 08 Jul 2002 to 128.112.82.136. Redistribution subject to AIP license or copyright, see http://ojps.aip.org/japo/japcr.jsp

TABLE IX. Material case 9, plane stress.

$G_2/G_1=0$, $G_1/K_1=0.37$, $G_2/K_2=1.5$, $\nu_1=0.33$, $\nu_2=0.0$ (3D Moduli) $G_2/G_1=0$, $G_1/k_1=0.50$, $G_2/k_2=1.0$, $\nu_1=0.33$, $\nu_2=0.0$ (2D Moduli) ϕ_2	$k_L^{(3)}/k_1$	k_e/k_1	$k_U^{(3)}/k_1$	$G_L^{(3)}/G_1$	G_e/G_1	$G_U^{(3)}/G_1$	ν_e	E_e/E_1
0.1	0.743	0.750	0.750	0.026	0.750	0.750	0.33	0.750
0.2	0.266	0.571	0.571	0.000	0.569	0.570	0.34	0.570
0.3	0.021	0.438	0.438	0.000	0.426	0.434	0.35	0.430
0.4	0.002	0.333	0.333	0.000	0.304	0.324	0.37	0.313
0.5	0.000	0.249	0.250	0.000	0.200	0.234	0.43	0.214
0.6	0.000	0.180	0.181	0.000	0.116	0.160	0.51	0.131
0.7	0.000	0.121	0.123	0.000	0.054	0.106	0.64	0.066
0.8	0.000	0.069	0.072	0.000	0.016	0.062	0.79	0.022
0.85	0.000	0.043	0.048	0.000	0.006	0.042	0.88	0.008

on a convergence study of sucessively finer boundary element meshes. The results correspond to the 926 node mesh described above.

Figure 3 shows the effective bulk modulus as a function of fiber volume fraction for the case of equal phase shear moduli and incompressible fibers (Table VI). In this case the bounds collapse yielding the exact result (34). Note the excellent agreement between the numerical results and the exact theoretical results.

Figure 4 shows the effective bulk modulus for the moderate case $G_2/G_1=6.75$, $\nu_1=0.35$, $\nu_2=0.20$ (Table IV). Here the three-point bounds are extremely tight up to near close packing. The numerical results lie between the bounds as required. The two-point bounds are not presented because they are close to the three-point bounds in this instance.

Figure 5 shows the effective bulk modulus for the glass-epoxy case $G_2/G_1=22.5$, $\nu_1=0.35$, $\nu_2=0.20$ (Table III). Here we show both two-point and three point bounds. It is clear that the three-point lower bound provides a very good estimate of k_e, consistent with the observations of Torquato.[6] We note that the Kantor–Bergman expansion[21] for the bulk modulus agrees very well with the simulation data of Fig. 5. Figure 6 shows the effective shear modulus for the same properties as in Fig. 5. Here we show both two-point and three-point bounds. Again the three-point lower bound provides a very good estimate of G_e. The Kantor–Bergman expansion for the shear modulus gives a reasonably good estimate of the data, but not as good as the agreement found in the corresponding case for the bulk modulus.

Figure 7 shows the effective shear modulus for the case of superrigid, incompressible fibers in an incompressible matrix, i.e., $G_2/G_1=\infty$, $\nu_1=\nu_2=0.50$ (Table V). The extreme shear modulus ratio and incompressibility provide a very stringent test of the numerical method. We only plot lower bounds here since the upper bounds diverge in this case. The three-point lower bound provides a good estimate of the data for a wide range of fiber volume fractions but appreciably underestimates the actual behavior at high volume fractions. Also shown are asymptotic results which hold in the dilute limit ($\phi_2 \ll 1$) and in the close-packing limit ($\phi_2 \simeq 0.91$) [cf. Eqs. (9) and (16)]. The numerical results are in very close agreement with these asymptotic results. We note that the Kantor–Bergman expansion for G_e deviates appreciably from the data at high cylinder volume fractions. Figure 8 shows the effective Poisson's ratio for the case of holes when the matrix Poisson's ratio is

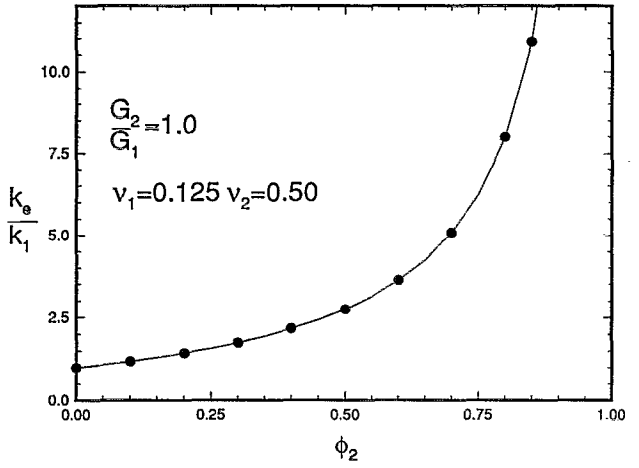

FIG. 3. Normalized effective bulk modulus k_e/k_1 vs cylinder volume fraction ϕ_2 for material case 6; —three-point bounds. The black circles are BEM results.

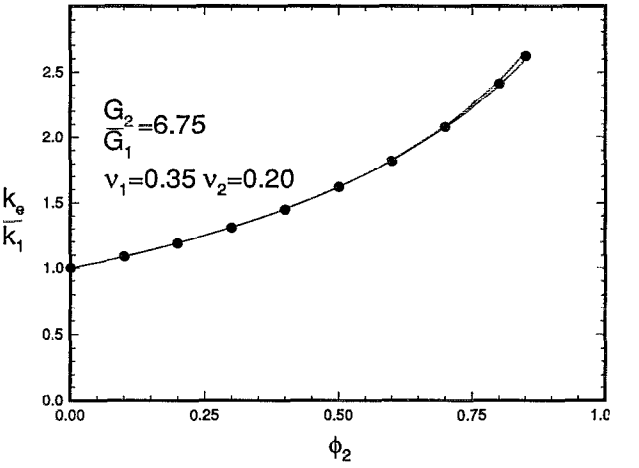

FIG. 4. Normalized effective bulk modulus k_e/k_1 vs cylinder volume fraction ϕ_2 for material case 4; —three-point bounds. The black circles are BEM results.

Downloaded 08 Jul 2002 to 128.112.82.136. Redistribution subject to AIP license or copyright, see http://ojps.aip.org/japo/japcr.jsp

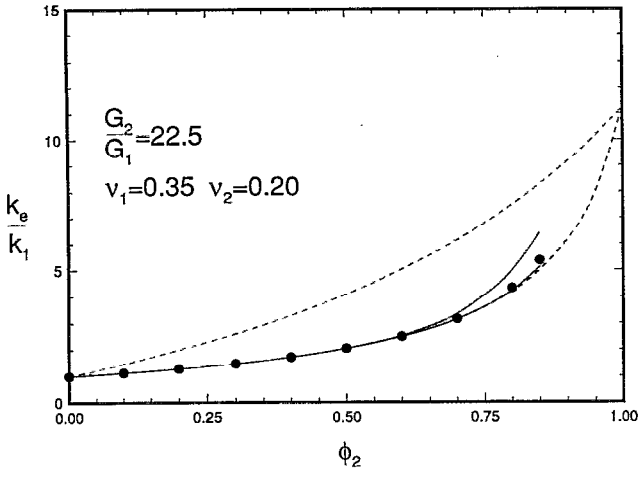

FIG. 5. Normalized effective bulk modulus k_e/k_1 vs cylinder volume fraction ϕ_2 for material case 3; --- two-point bounds; —three-point bounds. The black circles are BEM results.

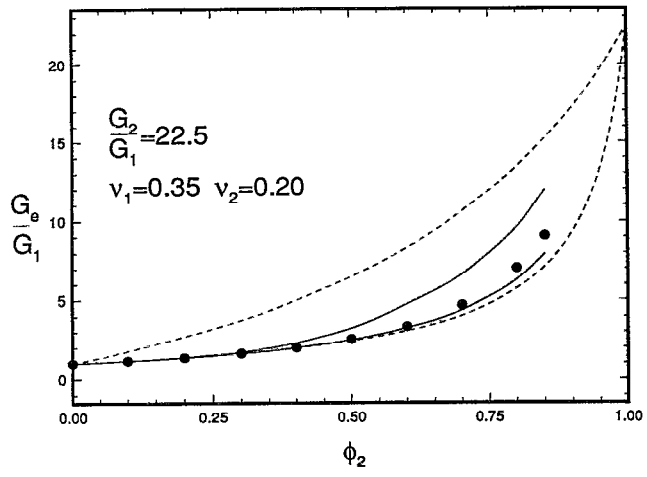

FIG. 6. Normalized effective shear modulus G_e/G_1 vs cylinder volume fraction ϕ_2 for material case 3; --- two-point bounds; —three-point bounds. The black circles are BEM results.

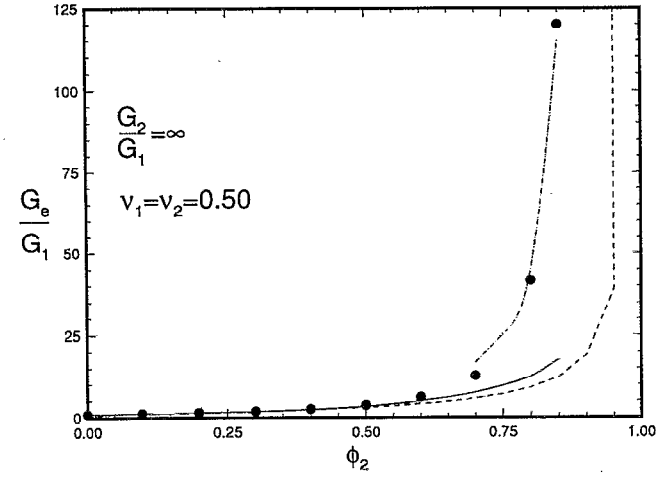

FIG. 7. Normalized effective shear modulus G_e/G_1 vs cylinder volume fraction ϕ_2 for material case 5; --- two-point lower bound; —three-point lower bound; ·-· asymptotic results Eqs. (9) and (16). The black circles are BEM results. On the scale of this figure, the dilute asymptotic result and the lower bounds are indistinguishable for small ϕ_2.

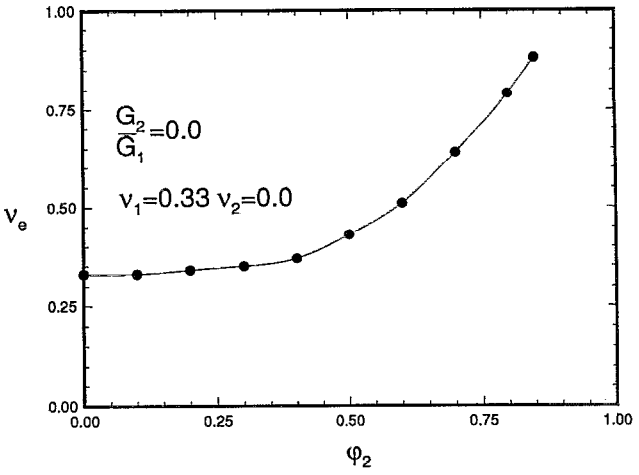

FIG. 8. Effective Poisson's ratio ν_e vs cylinder volume fraction ϕ_2 for material case 9 (plane stress hole case). The black circles are BEM results.

equal to 0.33 (Table IX). It appears that ν_e is approaching 1.0 in the close-packing limit, consistent with the results of Day *et al.*[16] who implicitly examined plane-strain elasticity.

Figure 9 shows the effective shear modulus for the case of holes for an incompressible matrix (Table VIII). The three-point upper bound is seen to be a relatively good predictor of the effective property, even at high volume fractions. The asymptotic results for the dilute and close-packing limit [cf. Eqs. (9) and (15)] are also shown. We note that the corresponding scaled effective Young's modulus E_e/E_1 in this case of holes is the same as E_e/E_1 for the previous case of holes (Table IX), i.e., E_e/E_1 is independent of the matrix Poisson's ratio. This observation was first made by Day *et al.*[16]

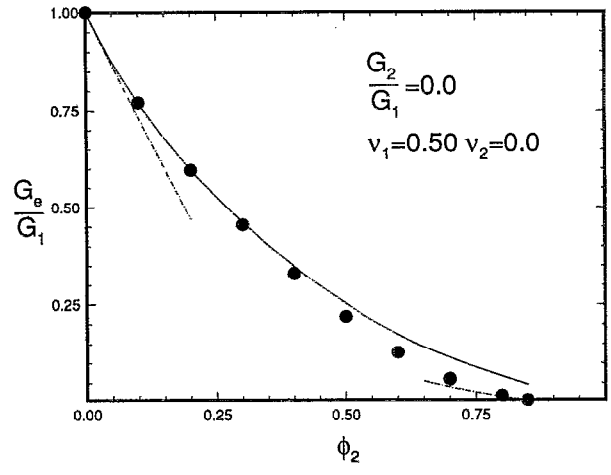

FIG. 9. Normalized effective shear modulus G_e/G_1 vs cylinder volume fraction ϕ_2 for material case 8; —three-point upper bound; ·-· asymptotic results Eqs. (9) and (15). The black circles are BEM results.

Downloaded 08 Jul 2002 to 128.112.82.136. Redistribution subject to AIP license or copyright, see http://ojps.aip.org/japo/japcr.jsp

V. CONCLUDING REMARKS

This paper demonstrates the utility of the boundary element method to efficiently and accurately compute the effective elastic moduli of composites. To illustrate the method we computed the elastic moduli of hexagonal arrays of cylinders or disks. We provided the most comprehensive set of effective-moduli data for this model and along the way calculated the three-point parameter η_2 for the first time. In a future study, we will apply the simulation technique to compute the effective elastic moduli of random arrays of cylinders (disks).

ACKNOWLEDGMENTS

The authors thank Y. Kantor for supplying them with an Erratum for Ref. 21. S.T. acknowledges the support of the Air Force Office of Scientific research under Grant No. F49620-92-J-0501. Some computer resources (CRAY Y-MP) were supplied by the North Carolina Supercomputing Center funded by the State of North Carolina.

APPENDIX: INTERRELATIONS AMONG THE 2D AND 3D ELASTIC MODULI

1. Single-phase interrelations

Consider a d-dimensional, linear, isotropic homogeneous material with bulk, shear, Young's modulus, and Poisson's ratio denoted by $K^{(d)}$, $G^{(d)}$, $E^{(d)}$, and $\nu^{(d)}$, respectively. (Note that in the text we let $k=K^{(2)}$ and $K=K^{(3)}$). The d-dimensional strain-stress relations are expressed as

$$\epsilon_{ij}=\frac{1}{E^{(d)}}\left[(1+\nu^{(d)})\sigma_{ij}-\nu^{(d)}\sigma_{kk}\delta_{ij}\right], \quad i,j,k=1,\ldots,d. \tag{A1}$$

The d-dimensional stress-strain relations are given by

$$\sigma_{ij}=(K^{(d)}-2G^{(d)}/3)\epsilon_{kk}\delta_{ij}+2G^{(d)}\epsilon_{ij}, \quad i,j,k=1,\ldots,d. \tag{A2}$$

We connect the 3D moduli to the 2D moduli by assuming either plane-strain or plane-stress elasticity. For plane-strain elasticity, we take $\epsilon_{11}=\epsilon_{12}=\epsilon_{13}=0$ in the relation (A1) with $d=3$. If we compare this simplified 3D expression to relation (A1) with $d=2$, we find the interrelations

$$E^{(2)}=\frac{E^{(3)}}{(1-\nu^{(3)})(1+\nu^{(3)})}, \tag{A3}$$

$$\nu^{(2)}=\frac{\nu^{(3)}}{1-\nu^{(3)}}. \tag{A4}$$

Similarly, by comparing Eq. (A2) with $d=3$ under plane-strain conditions and Eq. (A2) with $d=2$, we find

$$K^{(2)}=K^{(3)}+G^{(3)}/3, \tag{A5}$$

$$G^{(2)}=G^{(3)}. \tag{A6}$$

For plane-stress elasticity, we take $\sigma_{11}=\sigma_{12}=\sigma_{13}=0$ in the expression (A1) with $d=3$. Comparing this simplified 3D relation to relation (A1) with $d=2$ gives

$$E^{(2)}=E^{(3)}, \tag{A7}$$

$$\nu^{(2)}=\nu^{(3)}. \tag{A8}$$

Finally, comparing Eq. (A2) with $d=3$ under plane-stress conditions and Eq. (A2) with $d=2$, yields

$$K^{(2)}=\frac{9K^{(3)}G^{(3)}}{3K^{(3)}+4G^{(3)}}, \tag{A9}$$

$$G^{(2)}=G^{(3)}. \tag{A10}$$

Note that the interrelations derived above for homogeneous materials do not hold for the effective properties.

2. Effective plane-strain interrelations

The stress-strain relationships for a transversely isotropic composite material are

$$\bar{\epsilon}_{11}=\frac{1}{E_e}(\bar{\sigma}_{11}-\nu_e\bar{\sigma}_{22})-\frac{\nu_e^L}{E_e^L}\bar{\sigma}_{33}, \tag{A11}$$

$$\bar{\epsilon}_{22}=\frac{1}{E_e}(\bar{\sigma}_{22}-\nu_e\bar{\sigma}_{11})-\frac{\nu_e^L}{E_e^L}\bar{\sigma}_{33}, \tag{A12}$$

$$\bar{\epsilon}_{33}=-\frac{\nu_e^L}{E_e^L}(\bar{\sigma}_{11}+\bar{\sigma}_{22})+\frac{1}{E_e^L}\bar{\sigma}_{33}, \tag{A13}$$

$$\bar{\epsilon}_{12}=\frac{\bar{\sigma}_{12}}{2G_e}, \quad \bar{\epsilon}_{13}=\frac{\bar{\sigma}_{13}}{2G_e^L}, \quad \bar{\epsilon}_{23}=\frac{\bar{\sigma}_{23}}{2G_e^L}, \tag{A14}$$

where E_e, G_e, and ν_e are the transverse effective Young's modulus, shear modulus, and Poisson's ratio, while E_e^L, G_e^L, and ν_e^L are the corresponding properties for the longitudinal direction, respectively. There are five independent effective elastic moduli and hence there are interrelations among the moduli appearing in the above relations. For example,

$$G_e=\frac{E_e}{2(1+\nu_e)}, \quad E_e=4\left(\frac{1}{G_e}+\frac{1}{k_e}+\frac{4(\nu_e^L)^2}{E_e^L}\right)^{-1}, \tag{A15}$$

where k_e the effective transverse bulk modulus (without axial extension).

For any transversely isotropic two-phase fiber-reinforced material, Hill[19] has shown that there are only three independent effective elastic moduli since

$$E_e^L=\langle E\rangle+\frac{4(\nu_2-\nu_1)^2}{\left(\frac{1}{k_2}-\frac{1}{k_1}\right)^2}\left(\left\langle\frac{1}{k}\right\rangle-\frac{1}{k_e}\right), \tag{A16}$$

$$\nu_e^L=\langle\nu\rangle-\frac{(\nu_2-\nu_1)}{\frac{1}{k_2}-\frac{1}{k_1}}\left(\left\langle\frac{1}{k}\right\rangle-\frac{1}{k_e}\right). \tag{A17}$$

Downloaded 08 Jul 2002 to 128.112.82.136. Redistribution subject to AIP license or copyright, see http://ojps.aip.org/japo/japcr.jsp

3. Effective plane-stress interrelations

After some reflection, it is clear that the effective plane-strain moduli (denoted here by k_e, G_e, $\underset{\sim}{E}_e$, and $\underset{\sim}{\nu}_e$) and the plane-stress moduli (denoted here by $\tilde{k}_e$, $\tilde{G}_e$, $\tilde{E}_e$, and $\tilde{\nu}_e$) are generally not the same. For example, the effective plane-strain bluk modulus depends upon the phase moduli of the individual phases, i.e.,

$$k_e = f(k_1, k_2, G_1, G_2). \tag{A18}$$

The solution of the plane-stress problem is identical to the plane-strain problem except the former involves dependence upon the plane-stress phase moduli, i.e.,

$$\tilde{k}_e = f(\tilde{k}_1, \tilde{k}_2, \tilde{G}_1, \tilde{G}_2). \tag{A19}$$

Although the phase plane-strain and plane-stress shear moduli are the same [cf. Eqs. (A6) and (A10)], the phase plane-strain and plane-stress bulk moduli are different [cf. Eqs. (A5) and (A9)] and hence Eqs. (A18) and (A19) are generally not equal.

The derivation of the interrelations for the effective plane-strain and plane-stress moduli is too involved to place in the Appendix but will be the subject of a future investigation. Here we will only state the interrelations for the special case when one of the phases are *voids or holes* since we only examine plane-stress elasticity in our simulations in such instances. If phase 2 consists of voids or holes, then

$$\frac{1}{\tilde{k}_e} = \frac{1}{k_e} + \frac{4(\nu_e^L)^2}{E_e^L}, \tag{A20}$$

$$\frac{\tilde{E}_e}{\tilde{E}_1} = \frac{E_e}{E_1}, \tag{A21}$$

where ν_e^L and E_e^L were defined in Appendix 2.

[1] J. C. Maxwell, *Treatise on Electricity and Magnetism* (Clarendon, Oxford, 1873).
[2] Lord Rayleigh, Philos. Mag. **34**, 481 (1892).
[3] A. Einstein, Ann. Phys. **19**, 289 (1906).
[4] D. J. Bergman, Phys. Rep. C **43**, 377 (1978); G. W. Milton, J. Appl. Phys. **52**, 5294 (1981); G. W. Milton and N. Phan-Thien, Proc. R. Soc. London Ser. A **380**, 305 (1982); Y. Kantor and D. J. Bergman, J. Mech. Phys. Solids **32**, 41 (1984); S. Torquato, J. Chem. Phys. **84**, 6345 (1986); G. W. Milton and R. V. Kohn, J. Mech. Phys. Solids **36**, 597 (1988); J. Rubinstein and S. Torquato, J. Fluid Mech. **206**, 25 (1989).
[5] G. W. Milton, J. Mech. Phys. Solids **30**, 177 (1982).
[6] S. Torquato, Appl. Mech. Rev. **44**, 37 (1991).
[7] G. W. Milton, in *Homogenization and Effective Moduli of Materials and Media*, edited J. L. Eriksen, D. Kinderleher, R. Kohn, and J. L. Lions (Springer, New York, 1986).
[8] A. N. Norris, Mech. Mat. **4**, 1 (1985).
[9] K. A. Lurie and A. V. Cherkaev, J. Opt. Th. Appl. **46**, 571 (1985).
[10] G. A. Francfort and F. Murat, Archives Rat. Mech. Analy. **94**, 307 (1986).
[11] S. Torquato and G. Stell, J. Chem. Phys. **82**, 980 (1985); S. Torquato, and F. Lado, J. Phys. A **18**, 141 (1985); S. Torquato, J. Status Phys. **45**, 843 (1986); S. Torquato, J. Chem. Phys. **85**, 4622 (1986); N. A. Seaton and E. D. Glandt, *ibid.* **85**, 5262 (1986); S. Torquato, B. Lu, and J. Rubinstein, Phys. Rev. A **41**, 2059 (1990); G. Stell, in *Lectures in Applied Mathematics*, edited by W. Kohler and B. White (American Mathematical Society, RI, 1991), Vol. 27; B. Lu and S. Torquato, Phys. Rev. A **43**, 2078 (1991).
[12] S. Torquato and I. C. Kim, Appl. Phys. Lett. **55**, 1847 (1989). I. C. Kim and S. Torquato, J. Appl. Phys. **68**, 3892 (1990); **69**, 2280 (1991); **71**, 2727 (1992).
[13] D. F. Adams and D. R. Doner, J. Compos. Mater. **1**, 152 (1967).
[14] J. E. Flaherty and J. B. Keller, Common Pure and Appl. Math. **26**, 565 (1973).
[15] C. H. Chen and S. Cheng, J. Compos. Mater. **1**, 30 (1967).
[16] A. R. Day, K. A. Snyder, E. J. Garboczi, and M. F. Thorpe, J. Mech. Phys. Solids **40**, 1031 (1992).
[17] K. A. Snyder, E. J. Garboczi, and A. R. Day (unpublished).
[18] A. A. Becker, *The Boundary Element Method in Engineering* (McGraw–Hill, New York, 1992).
[19] J. W. Eischen and S. Torquato (to be published).
[20] See for example, T. S. Chow, and J. J. Hermans, J. Compos. Mater. **3**, 382 (1969).
[21] Y. Kantor and D. J. Bergman, J. Mech. Phys. Solids **30**, 355 (1982). The expression for the effective shear modulus Ge of a hexagonal array of cylinders given in this paper contains typographical errors. The correct expression is found in Y. Kantor, "Investigation of the Effective Elastic Properties of Composite Materials," Ph.D. dissertation, Tel-Aviv University, Israel, 1983.
[22] Z. Hashin and S. Shtrikman, J. Mech. Phys. Solids **11**, 127 (1963).
[23] R. Hill, J. Mech. Phys. Solids **12**, 199 (1964).
[24] Z. Hashin, J. Mech. Phys. Solids **13**, 119 (1965); Z. Hashin, in *Mechanics of Composite Materials* (Pergamon, New York, 1970).
[25] N. Silnutzer, Ph.D. thesis, University of Pennsylvania, PA, 1972.
[26] M. F. Thorpe and I. Jasiuk (unpublished).
[27] R. C. McPhedran and G. W. Milton, Appl. Phys. A **26**, 207 (1981).

Downloaded 08 Jul 2002 to 128.112.82.136. Redistribution subject to AIP license or copyright, see http://ojps.aip.org/japo/japcr.jsp